

The Effelsberg survey of FU Orionis and EX Lupi objects II. H₂O maser observations

Zs. M. Szabó^{1,2,3,4,*}, Y. Gong¹, W. Yang¹, K. M. Menten¹, O. S. Bayandina⁵, C. J. Cyganowski², Á. Kóspál^{3,4,6,7}, P. Ábrahám^{3,4,6}, A. Belloche¹ and F. Wyrowski¹

¹ Max-Planck-Institut für Radioastronomie, Auf dem Hügel 69, 53121 Bonn, Germany

e-mail: zszabo@mpi-fr-bonn.mpg.de

² Scottish Universities Physics Alliance (SUPA), School of Physics and Astronomy, University of St Andrews, North Haugh, St Andrews, KY16 9SS, UK

³ Konkoly Observatory, Research Centre for Astronomy and Earth Sciences, Eötvös Loránd Research Network (ELKH), Konkoly-Thege Miklós út 15-17, 1121 Budapest, Hungary

⁴ CSFK, MTA Centre of Excellence, Budapest, Konkoly Thege Miklós út 15-17., H-1121, Hungary

⁵ INAF - Osservatorio Astrofisico di Arcetri, Largo E. Fermi 5, 50125 Firenze, Italy

⁶ ELTE Eötvös Loránd University, Institute of Physics, Pázmány Péter sétány 1/A, H-1117 Budapest, Hungary

⁷ Max-Planck-Institut für Astronomie, Königstuhl 17, D-69117 Heidelberg, Germany

Received ; accepted

ABSTRACT

Context. FU Orionis (FUor) and EX Lupi (EXor) type objects are two groups of peculiar and rare pre-main sequence low-mass stars that are undergoing powerful accretion outbursts during their early stellar evolution. Though water masers are widespread in star forming regions and are powerful probes of mass accretion and ejection on small scales, little is known about the prevalence of water masers toward FUors and EXors.

Aims. We aim to perform the first systematic search for the 22.2 GHz water maser line in FUors and EXors in order to determine its overall incidence in these eruptive variables and facilitate follow-up high angular resolution observations.

Methods. We used the Effelsberg 100-m radio telescope to observe the H₂O (6₁₆ – 5₂₃) transition at 22.2 GHz toward a sample of 51 eruptive young stellar objects.

Results. We detect 5 water masers in our survey; 3 are associated with eruptive stars, equivalent to a detection rate of ~6% for our sample of eruptive sources. These detections include one EXor, V512 Per (also known as SVS 13 or SVS 13A), and two FUors, Z CMa and HH 354 IRS. This is the first reported detection of water maser emission towards HH 354 IRS. We also detect water maser emission in our pointing towards the FUor binary RNO 1B/1C, which most likely originates from the nearby deeply embedded source IRAS 00338+6312 (~4'' from RNO 1B/1C). Emission was also detected from H₂O(B) (also known as SVS 13C), a Class 0 source ~30'' from the EXor V512 Per. The peak flux density of H₂O(B) in our observations, 498.7 Jy, is the highest observed to date, indicating that we have serendipitously detected a water maser flare in this source. In addition to the two non-eruptive Class 0 sources (IRAS 00338+6312 and H₂O(B)/SVS 13C), we detect maser emission towards one Class 0/I (HH 354 IRS) and two Class I (V512 Per/SVS 13A and Z CMa) eruptive stars.

Conclusions. Despite the low detection rate, we demonstrate the presence of 22.2 GHz water maser emission in both FUor and EXor systems, opening the way to radio interferometric observations to study the environments of these eruptive stars on small scales. Comparing our data with historical observations spanning several decades suggests that multiple water maser flares have occurred in both V512 Per and H₂O(B).

Key words. Stars: pre-main sequence – Stars: low-mass – Stars: Formation – Masers – Stars: individual: V512 Per (V* 512 Per, SVS 13A, VLA 4) – Stars: individual: RNO 1B/1C – Stars: individual: IRAS 00338+6312 – Stars: individual: Z CMa – Stars: individual: HH 354 IRS

1. Introduction

Low-mass young stellar objects (YSOs) are stars in the early stages of stellar evolution, specifically protostars and pre-main sequence (PMS) stars, which can undergo accretion-driven episodic outbursts. Studies of outbursting objects provide crucial information on the formation and the evolution of Sun-like stars. Amongst PMS stars, there are two small, but rather spectacular classes of outbursting low-mass YSOs: FU Orionis and

EX Lupi-type stars (FUors and EXors for short, respectively). Members of both classes show major increases in their optical and near-infrared (NIR) brightnesses. FUors can brighten by up to 5 – 6 magnitudes in the optical, triggered by enhanced accretion from the accretion disk onto the protostar (Hartmann & Kenyon 1996; Herbig 1989). This phase can last for several decades, or even centuries (e.g. the recent review by Fischer et al. 2022, and references therein). For example, the prototype of the FUor class, FU Orionis, went into outburst in 1936 (Wachmann 1954), and remains in a highly active state. After a few other objects were observed to experience similar outbursts, Herbig (1977) defined the FUor class, which continues to increase in

* Member of the International Max Planck Research School (IMPRS) for Astronomy and Astrophysics at the Universities of Bonn and Cologne.

size as new FUor-type objects are identified (e.g., Audard et al. 2014; Szegedi-Elek et al. 2020) and currently contains more than a dozen objects. The EXor class was defined by Herbig (1989), based on the properties of the prototype star EX Lupi, and currently also includes more than a dozen objects (e.g., Audard et al. 2014; Park et al. 2022). EXors can brighten by up to 1 – 5 magnitudes in the optical and remain in a bright state for a few months or a few years (see e.g., Jurdana-Šepić et al. 2018); furthermore, their outbursts are recurring (e.g., Audard et al. 2014; Cruz-Sáenz de Miera et al. 2022).

Interstellar masers are powerful tools for studying the physics of star formation on small scales, frequently probing regions of enhanced density and temperature (e.g., Elitzur 1992; Reid & Honma 2014). While masers have been substantially used to probe both low- and high-mass star formation regions (e.g., Abraham et al. 1981; Omodaka et al. 1999; Hirota et al. 2011; Furuya et al. 2001, 2003), so far little information exists on masers in FUors/EXors. Pioneering studies found compact maser emission in the 1720 MHz hyperfine structure line of hydroxyl (OH) toward the archetypal FUor V1057 Cyg (Lo & Bechis 1973). This emission, which comes from the immediate vicinity of the star (Lo & Bechis 1974) and is highly time variable (Winnberg et al. 1981), is unique in the literature. The 22.2 GHz transition of water (H₂O) is the most widespread interstellar maser (see, e.g., Gray 2012, and references therein). It has been detected towards numerous low- to high-mass star forming regions in the Milky Way (see e.g. Ladeyschikov et al. 2022). Pumping models indicate that 22.2 GHz water masers are excited at elevated temperatures (~500 K) and densities (10^{8-9} cm⁻³), which are typically found in the compressed post-shock regions of jets/outflows from YSOs (Elitzur et al. 1989a; Elitzur & Fuqua 1989; Gray 2012; Gray et al. 2022). With very-long-baseline interferometry (VLBI), multi-epoch observations of water masers associated with protostellar outflows can be used to study mass accretion and ejection (see, for example, Burns et al. 2016; Moscadelli et al. 2019). This suggests that water masers could potentially serve as valuable probes of mass accretion and ejection in FUors/EXors.

Despite the fact that water masers are closely associated with mass accretion and ejection in protostars, a systematic search for 22.2 GHz H₂O masers in FUors/EXors has not yet been performed. Hence, the overall incidence of 22.2 GHz water masers in these classes of eruptive objects is unknown. In this paper, we present the first dedicated 22.2 GHz water maser survey of low-mass young eruptive stars, using the Effelsberg 100-m telescope. Our single-dish survey is a first step in investigating water masers in low-mass outbursting systems, aimed at investigating the existence and prevalence of water masers in these objects and identifying targets for follow-up interferometric observations. This paper is the second in a series (the first being Szabó et al. 2023) presenting radio and (sub)millimeter observations of FUors and EXors and their natal environments, and is organized as follows. In Sect. 2, we summarize our observations. In Sect. 3, we present our results, focusing on sources with water maser detections. In Sect. 4, we discuss our results, and in Sect. 5 we summarize our most important findings.

2. Observations

The H₂O $J_{K_a, K_c} = 6_{16} - 5_{23}$ transition (rest frequency 22235.0798 MHz, from the JPL Molecular Spectroscopy database¹, Pickett et al. 1998) was observed simultaneously

with the three lowest metastable NH₃ transitions ($(J, K) = (1, 1), (2, 2)$ and $(3, 3)$), which were presented in Paper I (Szabó et al. 2023). The observations were carried out on 2021 November 18, November 23, and 2022 January 25 using the Effelsberg 100-m telescope in Germany² (project id: 95-21, PI: Szabó). The sample consisted of 51 sources: 33 FUors, 13 EXors, and 5 Gaia alerts. Gaia alert sources were chosen from the variable sources identified by the Gaia Photometric Science Alerts system (Hodgkin et al. 2021) based on light curve characteristics and luminosities similar to those of FUors/EXors. Five Gaia alert sources in our sample are yet to be classified; one source, Gaia18dvy, is listed with its Gaia alert name (Table B.1) but counted as a FUor based on its classification by Szegedi-Elek et al. (2020).

Our observations were performed in position-switching mode with an off-position at an offset of 5' east of our targets in azimuth. During our observations, the 1.3 cm double beam and dual polarization secondary focus receiver was employed as the frontend, while the Fast Fourier Transform Spectrometers (FFTSs) were used as the backend. Each FFTS provides a bandwidth of 300 MHz and 65536 channels, which gives a channel width of 4.6 kHz, corresponding to a velocity spacing of 0.06 km s⁻¹ at 22.2 GHz. The actual spectral resolution is coarser by a factor of 1.16 (Klein et al. 2012).

At the beginning of each observing session, pointing and focus were verified towards NGC 7027. On 2021 November 18 we also targeted W75N, known for its H₂O and NH₃ emission, to make sure that the system was working properly (see Appendix A). Pointing was regularly checked on nearby continuum sources, and was found to be accurate to about 5''. NGC 7027 was also used as our flux calibrator, assuming a flux density of ~5.6 Jy at 22.2 GHz (Ott et al. 1994). The on-source integration time was 2.5 minutes per spectrum, and during each observing epoch, 4 spectra per source were obtained.

The majority of our sources were observed on 2021 November 18 and 23 (see Tables 2 and B.1). On 2021 November 18, we detected H₂O maser emission toward V512 Per (SVS 13A), RNO 1B/1C, and HH 354 IRS. To study the time variability of the maser emission, we re-observed detected sources in as many subsequent epochs as possible (see Table 2), within the constraints of our allocated observing sessions. For Z CMA, which was known to have water maser emission (Moscadelli et al. 2006) but could not be observed in November 2021 due to time constraints, we searched for short-term maser variability by observing this source for two 4×2.5 minute blocks separated by 2.5 hours in January 2022. No variability was detected on this timescale, so all 8 spectra of Z CMA were averaged for the subsequent analysis. We note, that due to the weak detection of the water maser in HH 354 IRS, the spectrum was spectrally smoothed by a factor of 2 using the smooth built-in function in CLASS. The smoothed spectrum is presented throughout this paper. Having detected unusually high-amplitude (factor of ~4 with respect to the previous observation) and rapid variability in the H₂O maser spectra towards V512 Per (SVS 13A) (see Sect. 3.2.1), we also carried out nine-point observations and 1'×1' On-The-Fly (OTF) mapping of this source on 2022 February 5 to investigate whether emission from nearby sources in the telescope sidelobes could be contributing to the observed emission. Consequently, we serendipitously detected strong water maser emission toward H₂O(B) (SVS 13C), which is 30'' from V512 Per (SVS 13A)

² The 100-m telescope in Effelsberg is operated by the Max-Planck-Institut für Radioastronomie (MPIfR) on behalf of the Max-Planck-Gesellschaft (MPG).

¹ <https://spec.jpl.nasa.gov/>

(see Sect. 3.2.1 and 3.3.1). We also performed single-pointing observations towards H₂O(B) during this epoch.

We adopted the method introduced by Winkel et al. (2012) for our spectral calibration which resulted in a calibration uncertainty of about 15%. The half-power beam width (HPBW) was about 40'' at 22 GHz and the main beam efficiency was 60.2% at 22 GHz. The conversion factor from flux density, S_ν , to main beam brightness temperature, T_{mb} , was $T_{\text{mb}}/S_\nu = 1.73$ K/Jy. Typical RMS noise levels for observations of detected sources are given in Table 2 and 3σ upper limits for non-detections are given in Table B.1.

The data were reduced using the GILDAS/CLASS package developed by the Institut de Radioastronomie Millimétrique (IRAM)³ (Pety 2005; Gildas Team 2013). For each target, spectra observed on the same day were averaged to improve the signal-to-noise ratio prior to subtracting a linear baseline. Velocities are presented with respect to the local standard of rest (LSR) throughout this paper.

3. Results

Of our 51 targets, we detected $>3\sigma$ water maser emission towards two FUors (Z CMA and HH 354 IRS) and one EXor (V512 Per/SVS 13A), corresponding to a detection rate of $\sim 6\%$ towards eruptive stars. We also serendipitously detected water maser emission towards two non-eruptive embedded protostars, which we discuss in Sects. 3.3.1 and 3.3.2. The basic parameters of sources with maser detections, including types, coordinates, distances, and evolutionary classifications are listed in Table 1. In all, we detected water masers in two non-eruptive Class 0 sources (IRAS 00338+6312 and H2O(B)/SVS 13C) and in one Class 0/I (HH 354 IRS) and two Class I (V512 Per/SVS 13A and Z CMA) eruptive objects, using the standard classification scheme (see, e.g., Greene et al. 1994; Evans et al. 2009).

For sources with water maser detections, we fitted each velocity component with a Gaussian to obtain its LSR velocity (v_{LSR}), line width (Δv), and peak flux density (S_ν), given in Table 2. The peak flux densities of detected water masers vary from 0.11 Jy to 498.7 Jy, spanning over 3 orders of magnitude. The observed maser velocities are within 10 km s^{-1} of the systemic cloud velocities measured from NH₃ emission. While shock velocities of $\geq 50 \text{ km s}^{-1}$ are expected in theoretical models (e.g., Elitzur et al. 1989b), the modest velocity offsets between water masers and dense gas observed in our sample are generally consistent with observations of water masers towards high-mass YSOs (e.g., Urquhart et al. 2009; Cyganowski et al. 2013, Fig. 4 and Fig. 16 respectively). Isotropic H₂O maser luminosities, $L_{\text{H}_2\text{O}}$, were calculated as (e.g., Anglada et al. 1996; Urquhart et al. 2011; Cyganowski et al. 2013):

$$\left[\frac{L_{\text{H}_2\text{O}}}{L_\odot} \right] = 2.3 \times 10^{-8} \left[\frac{\int S_\nu dv}{\text{Jy km s}^{-1}} \right] \left[\frac{D}{\text{kpc}} \right]^2, \quad (1)$$

where D is the distance to the target (see Table 1). Estimating the isotropic H₂O maser luminosities of individual velocity components separately, we find a range of $L_{\text{H}_2\text{O}}$ of $7.9 \times 10^{-10} L_\odot$ to $6.1 \times 10^{-7} L_\odot$ (see Table 2).

In the following subsections, we discuss our results for sources with detected water masers. Our non-detections are presented in Appendix B, where Table B.1 lists the targeted sources along with their types, coordinates, 3σ upper limits, whether they were previously searched for 22.2 GHz maser emission and

if so the reference, the date of observation in the current survey, their classification and reference, and distances.

For 31 sources in our sample, no previous observations of the 22.2 GHz water maser line have been reported in the literature.

3.1. FUors

3.1.1. Z CMA

Z CMA consists of an FUor (southwest component) and a Herbig Ae/Be star (northeast component) that are only 0.1'' apart (Koresko et al. 1991; Bonnefoy et al. 2017). Figure 1 shows the H₂O maser spectrum observed toward Z CMA, the only source among those detected observed at only one epoch (Sect. 2). As shown in Figure 1, there is only one bright maser feature, at $v_{\text{LSR}} = 7.82 \text{ km s}^{-1}$, blueshifted by $\sim 6 \text{ km s}^{-1}$ with respect to the thermal NH₃ emission. Although Z CMA has been observed in many previous water maser studies (Blitz & Lada 1979; Thum et al. 1981; Deguchi et al. 1989; Scappini et al. 1991; Palla & Prusti 1993; Moscadelli et al. 2006; Sunada et al. 2007; Bae et al. 2011; Kim et al. 2018), maser emission was detected only on 2003 March 14 (Moscadelli et al. 2006), with a flux density of $\sim 2 \text{ Jy}$ at $v_{\text{LSR}} = 14.3 \text{ km s}^{-1}$. The maser component at $v_{\text{LSR}} = 7.82 \text{ km s}^{-1}$ is reported here for the first time.

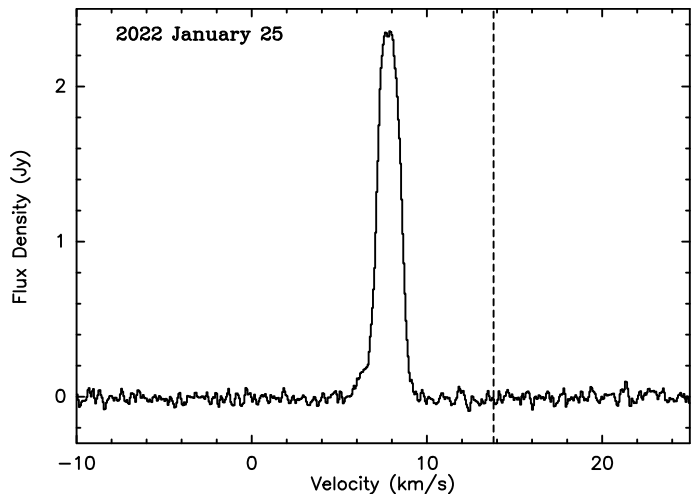


Fig. 1: H₂O maser spectrum of Z CMA observed on 2022 January 25. The dashed vertical line indicates the v_{LSR} of 13.8 km s^{-1} from the NH₃ (1,1) transition (Szabó et al. 2023).

3.1.2. HH 354 IRS

HH 354 IRS, also known as IRAS 22051+5848 and L1165-SMM1 (e.g., Visser et al. 2002), was classified as a FUor based on its CO first-overtone bandhead feature at $\sim 2.3 \mu\text{m}$ (Reipurth & Aspin 1997; Connelley & Reipurth 2018). This FUor was searched for H₂O maser emission multiple times between 1985 and 2005 (Wouterloot et al. 1993; Persi et al. 1994; Sunada et al. 2007), but no maser emission was reported.

As shown in Figure 2, we detected weak H₂O maser emission (peak flux densities $< 0.2 \text{ Jy}$, Table 2) towards HH 354 IRS in two epochs. These are the first detections of water maser emission towards this source. On 2021 November 18, we detected a weak H₂O maser at $v_{\text{LSR}} = 1.18 \text{ km s}^{-1}$. On 2022 January 25 we detected two features at $v_{\text{LSR}} = -10.51$ and $v_{\text{LSR}} = 5.04 \text{ km s}^{-1}$ but the 1.18 km s^{-1} feature had disappeared. This variability is

³ <https://www.iram.fr/IRAMFR/GILDAS/>

Table 1: Basic information about the sources towards which water maser emission was detected at 22.2 GHz.

Name	Type FUor/EXor	R.A. (J2000) (^h ^m ^s)	Dec. (J2000) ([°] ['] ^{''})	Distance (pc)	Classification	Reference
Z CMa	FUor	07 03 43.15	−11 33 06.2	1125	Class I	1, 2, 3
HH 354 IRS	FUor	22 06 50.37	+59 02 45.9	750	Class 0/I	1, 4, 5, 6
V512 Per (SVS 13A)	EXor	03 29 03.75	+31 16 03.9	275	Class I	1, 7, 8
IRAS 00338+6312 (close to RNO 1B/1C)	−	00 36 46.30	+63 28 54.0	965	Class 0	7, 9
H ₂ O(B) (SVS 13C)*	−	03 29 01.35	31 15 40.4	275	Class 0	7, 10

Notes. *The coordinates given for H₂O(B) were derived from the OTF mapping.

References for distance and classification: 1 – Audard et al. (2014); 2 – Dong et al. (2022); 3 – Gramajo et al. (2014); 4 – Reipurth et al. (1997); 5 – Bronfman et al. (1996); 6 – Reipurth et al. (1997); 7 – Bailer-Jones et al. (2021); 8 – Diaz-Rodriguez et al. (2022); 9 – Quanz et al. (2007); 10 – Plunkett et al. (2013).

Table 2: Properties of observed water maser features.

Source	Date yyyy-mm-dd	H ₂ O					NH ₃ (1,1)
		v_{LSR} (km s ^{−1})	Δv (km s ^{−1})	RMS (Jy)	S_{ν} (Jy)	$L_{\text{H}_2\text{O}}$ (L_{\odot})	v_{LSR} (km s ^{−1})
V512 Per (SVS 13A)*	2021-11-18	6.31 (0.06)	1.20 (0.06)	0.07	20.20 (0.07)	3.7×10^{-8}	
V512 Per*	2021-11-18	8.46 (0.06)	0.86 (0.06)	0.07	19.24 (0.07)	3×10^{-8}	
V512 Per*	2021-11-18	10.91 (0.06)	0.74 (0.06)	0.07	19.02 (0.07)	2.4×10^{-8}	8.45 (0.01)
V512 Per*	2021-11-18	11.68 (0.06)	0.56 (0.06)	0.07	16.88 (0.07)	1.6×10^{-8}	
V512 Per*	2021-11-18	13.23 (0.06)	1.56 (0.06)	0.07	1.72 (0.07)	3.6×10^{-9}	
V512 Per*	2021-11-23	6.30 (0.03)	1.08 (0.01)	0.04	55.81 (0.05)	9.7×10^{-8}	
V512 Per*	2021-11-23	8.42 (0.03)	0.95 (0.01)	0.04	86.38 (0.05)	1.5×10^{-7}	
V512 Per*	2021-11-23	10.95 (0.03)	0.81 (0.01)	0.04	16.14 (0.05)	2.8×10^{-8}	8.45 (0.01)
V512 Per*	2021-11-23	11.11 (0.03)	1.28 (0.01)	0.04	15.85 (0.05)	3.1×10^{-8}	
V512 Per*	2021-11-23	13.40 (0.03)	0.88 (0.01)	0.04	2.91 (0.05)	4.1×10^{-9}	
V512 Per*	2022-02-05	5.15 (0.01)	0.74 (0.03)	0.06	2.09 (0.01)	2.8×10^{-9}	
V512 Per*	2022-02-05	6.13 (0.01)	0.67 (0.01)	0.06	21.31 (0.01)	2.7×10^{-8}	
V512 Per*	2022-02-05	7.21 (0.01)	0.69 (0.01)	0.06	4.33 (0.01)	5.3×10^{-9}	8.45 (0.01)
V512 Per*	2022-02-05	8.63 (0.01)	0.97 (0.01)	0.06	7.99 (0.01)	1.4×10^{-8}	
V512 Per*	2022-02-05	9.64 (0.01)	1.12 (0.01)	0.06	5.81 (0.01)	1.2×10^{-8}	
V512 Per*	2022-02-05	11.82 (0.01)	1.11 (0.01)	0.06	2.49 (0.05)	4.5×10^{-9}	
H ₂ O(B) (SVS 13C)**	2022-02-05	5.07 (0.01)	0.63 (0.01)	0.06	41.45 (0.05)	4.8×10^{-8}	
H ₂ O(B)**	2022-02-05	6.14 (0.01)	0.66 (0.01)	0.06	498.7 (0.05)	6.1×10^{-7}	
H ₂ O(B)**	2022-02-05	7.22 (0.01)	0.76 (0.01)	0.06	98.30 (0.05)	1.3×10^{-7}	8.33 (0.01)
H ₂ O(B)**	2022-02-05	8.62 (0.01)	0.92 (0.01)	0.06	182.34 (0.05)	3.1×10^{-7}	
H ₂ O(B)**	2022-02-05	9.61 (0.01)	0.96 (0.01)	0.06	126.73 (0.05)	2.3×10^{-7}	
IRAS 00338+6312	2021-11-18	−28.78 (0.01)	1.72 (0.01)	0.05	2.61 (0.09)	1.1×10^{-7}	
IRAS 00338+6312	2021-11-18	−15.79 (0.05)	0.96 (0.05)	0.05	0.37 (0.09)	6.2×10^{-9}	
IRAS 00338+6312	2021-11-23	−28.78 (0.01)	1.70 (0.01)	0.04	2.75 (0.09)	1.1×10^{-7}	−17.90 (0.06)
IRAS 00338+6312	2021-11-23	−15.88 (0.02)	0.69 (0.05)	0.04	0.39 (0.09)	5.6×10^{-9}	
IRAS 00338+6312	2022-01-25	−28.48 (0.01)	1.75 (0.02)	0.04	1.10 (0.09)	4.1×10^{-8}	
IRAS 00338+6312	2022-02-05	−28.43 (0.01)	1.69 (0.02)	0.05	1.63 (0.09)	6.3×10^{-8}	
HH 354 IRS	2021-11-18	1.18 (0.06)	0.81 (0.10)	0.07	0.18 (0.03)	2.1×10^{-9}	
HH 354 IRS	2022-01-25	−10.51 (0.02)	0.54 (0.05)	0.02	0.11 (0.02)	7.9×10^{-10}	−1.52 (0.01)
HH 354 IRS	2022-01-25	5.04 (0.02)	0.63 (0.05)	0.02	0.18 (0.02)	1.6×10^{-9}	
Z CMa	2022-01-25	7.82 (0.01)	1.36 (0.01)	0.01	2.36 (0.01)	1.1×10^{-7}	13.8 (0.02)

Notes. * From pointed observations towards V512 Per; possible contamination by H₂O(B) is discussed in Sect. 3.3.1. **From pointed observations towards H₂O(B) (see also Sect. 3.3.1).

consistent with the findings of Claussen et al. (1996) that water maser features associated with low-mass YSOs can have lifetimes of $\lesssim 2$ months.

3.2. EXors

3.2.1. V512 Per (SVS 13A)

Located in the low-mass star-forming region NGC 1333, the source V512 Per (commonly known as SVS 13 or SVS 13A, e.g. Plunkett et al. 2013) has been the subject of extensive multiwavelength studies, resulting in a complex nomenclature. The source was discovered during an infrared survey (SVS76 NGC 1333 13A, Strom et al. 1976). An optical outburst

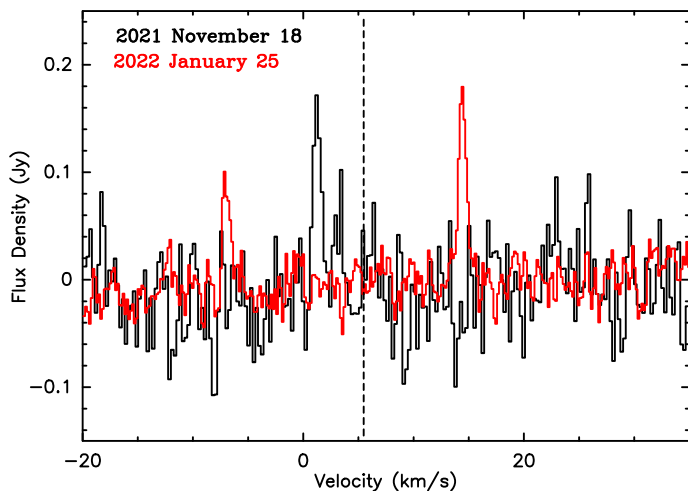


Fig. 2: Spectrally smoothed line profile of H₂O maser emission observed in HH 354 IRS on 2021 November 18 and 2022 January 25. The dashed vertical line indicates the average v_{LSR} of -1.47 km s^{-1} derived from the NH₃ (1,1) and (2,2) transitions (Szabó et al. 2023).

was detected in the late 1980’s (Mauro & Thouvenot 1991) and observations by Eisloffel et al. (1991) confirmed it showed EXor properties. The variable name V512 Per was assigned in the 71st Name-List of Variable Stars by Kazarovets et al. (1993), who noted SVS 13 and V512 Per were the same source. A radio counterpart of the optical/near-infrared source, named VLA 4, was first detected by Rodríguez et al. (1997) and later resolved into a binary (VLA 4A and 4B; Anglada et al. 2000). Rodríguez et al. (2002) note that SVS 13 (therefore V512 Per) and VLA 4 are the same source, consistent with other studies (see, e.g., Goodrich 1986; Fujiyoshi et al. 2015). The source is also commonly known as SVS 13A (see, e.g., Plunkett et al. 2013, and references therein) and is associated with several Herbig/Haro objects (HH 7–11; e.g., Rodríguez et al. 1997; Bachiller et al. 2000). In this paper we refer to the source as V512 Per, noting that this name might be more familiar to the variable star community (e.g., Kazarovets et al. 1993; Audard et al. 2014) while SVS 13, VLA 4, or SVS 13A may be more familiar to the radio astronomy community (e.g., Rodríguez et al. 2002; Plunkett et al. 2013).

Figure 3 shows the spectra obtained towards V512 Per in 2021 November. On 2021 November 18, we detected at least 6 maser features towards V512 Per (see Figure 3), with the brightest one being 20.2 Jy. Here we note that only 5 of them are shown in Table 2, since the additional feature on the main component at 6.31 km s^{-1} cannot result in a reliable Gaussian fit. Five days later, two velocity features, at 6.3 km s^{-1} and 8.4 km s^{-1} , had increased in flux density by factors of ~ 3 and ~ 4 , respectively. Previous H₂O maser observations of the V512 Per region revealed three maser positions, H₂O(A), H₂O(B), and H₂O(C) (Haschick et al. 1980). H₂O(A) is associated with V512 Per. H₂O(B), also known as HH 7-11(B), VLA 2, SVS 13C, or MMS3, is a Class 0 source located $\sim 0.5'$, to the southwest (Cesaroni et al. 1988; Segura-Cox et al. 2018; Chen et al. 2013; Plunkett et al. 2013), while H₂O(C) is $\sim 2.5'$ southeast of V512 Per (Haschick et al. 1980).

To investigate which of the observed velocity components may be associated with V512 Per, we carried out a nine-point grid of observations centred on V512 Per on 2022 February 5 (with pointings separated by $20''$). The results indicate that the

strong water maser features at $5\text{--}10 \text{ km s}^{-1}$ are brightest at an offset position ($-20'', -20''$) rather than toward V512 Per ($0'', 0''$), suggesting that these maser features do not arise mainly from V512 Per. The $\sim 12 \text{ km s}^{-1}$ component, in contrast, is strongest towards V512 Per and is likely associated with the eruptive source (Figure 4, see also Figure 5).

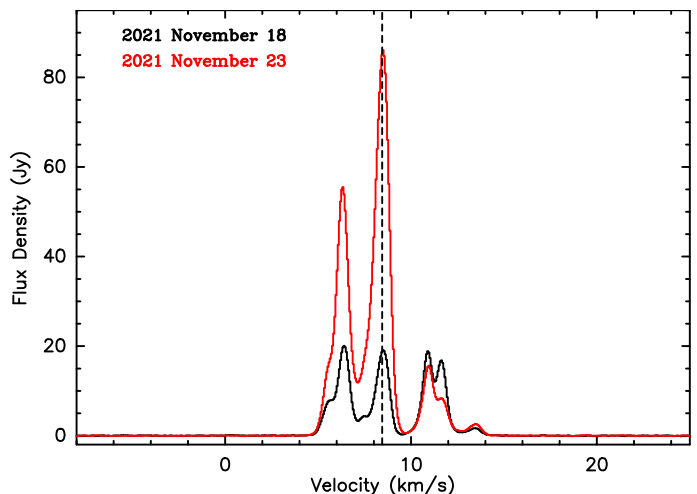


Fig. 3: H₂O maser spectra toward V512 Per in November 2021: the two epochs are indicated at upper left. The dashed line indicates the average v_{LSR} of 8.39 km s^{-1} derived from the NH₃ (1,1), (2,2) and (3,3) transitions (Szabó et al. 2023).

3.3. Serendipitous detections towards Class 0 protostars

3.3.1. A water maser flare in H₂O(B)

In addition to the nine-point map described above (Sect. 3.2.1), we also performed OTF mapping towards V512 Per and H₂O(B), shown in Figure 5. As illustrated by the channel maps in Figure 5, spectral features at $v_{\text{LSR}} \leq 11 \text{ km s}^{-1}$ peak around H₂O(B) while spectral features at $v_{\text{LSR}} > 11 \text{ km s}^{-1}$ peak around V512 Per. Figure 4 compares our pointed observations toward V512 Per and H₂O(B) on 2022 February 5: the spectra show very similar profiles between 4 km s^{-1} and $\sim 10 \text{ km s}^{-1}$ but the intensities are different by a factor of ~ 20 . This similarity suggests that our pointed observations of V512 Per, including those shown in Figure 3, have significant contributions from H₂O(B). We estimate this contribution for our 2022 February 5 observations assuming a perfect Gaussian beam pattern with a beam size of $40''$. A source at an offset of $38.7''$ (the angular separation between V512 Per and H₂O(B) derived from our observations, see Table 1) will fall at the 7.5% response level of the beam, or between the 3.7–14% levels assuming a typical pointing error of $5''$. Thus H₂O(B), with a flux density of 498.7 Jy, would contribute 18.4–69.8 Jy to the spectrum observed towards V512 Per, comparable to the observed value of 21.3 Jy (Table 2).

Notably, in our pointed 2022 February 5 observations, the peak flux density of the water maser in H₂O(B) is 498.7 Jy at $v_{\text{LSR}} = 6.1 \text{ km s}^{-1}$. This is the highest flux density reported for this source to-date (c.f. Haschick et al. 1980; Lyo et al. 2014), indicative of a maser flare (see also Sect. 4.1).

3.3.2. RNO 1B/1C and IRAS 00338+6312

RNO 1B/1C (V710 Cas) is a double FUor system, with both RNO 1B and 1C classified as FUors (Staudé & Neckel 1991;

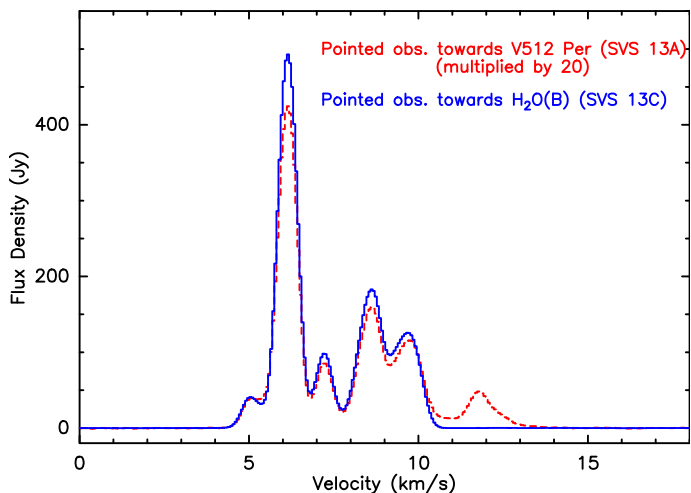


Fig. 4: Pointed H₂O maser spectra towards V512 Per and H₂O(B) observed on 2022 February 5. The spectrum of V512 Per is multiplied by 20 to better match the spectrum of H₂O(B).

Kenyon et al. 1993). The binary is part of a cluster of deeply embedded YSOs (e.g., Quanz et al. 2007) that has been targeted by numerous water maser studies (e.g., Fiebig 1995; Furuya et al. 2003; Sunada et al. 2007; Bae et al. 2011, and references therein). Previous VLA observations of the clustered region suggest that the water masers between $v_{\text{LSR}} \sim -30 \text{ km s}^{-1}$ and $v_{\text{LSR}} \sim -5 \text{ km s}^{-1}$ originate from the deeply embedded Class 0 object IRAS 00338+6312 rather than RNO 1B or RNO 1C (see, e.g., Fiebig 1995; Fiebig et al. 1996, and references therein). IRAS 00338+6312 is only $\sim 4''$ northeast of RNO 1C, but is a separate object (e.g., Mookerjee et al. 1999; Quanz et al. 2007). The blueshifted and redshifted masers are thought to arise from the bipolar outflow or an accretion disk (Fiebig et al. 1996).

In our pointing towards RNO 1B/1C, we detected water maser emission in four epochs, as shown in Figure 6. During our first observations on 2021 November 18, we detected two maser features at $v_{\text{LSR}} = -28.78 \text{ km s}^{-1}$ and $v_{\text{LSR}} = -15.79 \text{ km s}^{-1}$, and five days later the flux densities and LSR velocities of the two maser features were nearly unchanged. The source was observed again on 2022 January 25 and February 5: in these observations, the $v_{\text{LSR}} \sim -15.8 \text{ km s}^{-1}$ feature had disappeared and the blueshifted maser was weaker and had slightly shifted in velocity, to $v_{\text{LSR}} \sim -28.48 \text{ km s}^{-1}$. The 3σ upper limits for the $v_{\text{LSR}} \sim -15.8 \text{ km s}^{-1}$ feature are 0.12 Jy and 0.15 Jy for the observations on 2022 January 25 and February 5, respectively. We also note that the $v_{\text{LSR}} \sim -28 \text{ km s}^{-1}$ feature has the largest velocity offset with respect to the cloud among our detections, $\sim 10 \text{ km s}^{-1}$ (see Table 2). Based on comparing our results to the literature, the water maser features detected in our survey are most likely to originate from IRAS 00338+6312 rather than RNO 1B/1C. The velocities of our detected masers are similar to those of the masers associated with IRAS 00338+6312 in the VLA observations (Fiebig 1995; Fiebig et al. 1996), and also match the velocity range of the molecular outflow (about -30 km s^{-1} to -5 km s^{-1} Snell et al. 1990; Yang et al. 1991) driven by IRAS 00338+6312 (Henning et al. 1992; Wouterloot et al. 1993; Anglada et al. 1994; Furuya et al. 2003; Bae et al. 2011). We therefore do not count the water maser emission in our RNO 1B/1C pointing as a detection towards an eruptive star, and the 3σ upper limits are given in Table B.1.

4. Discussion

4.1. Long-term time variation

Water maser flares have been recognized in star forming regions for decades (e.g., Boboltz et al. 1998; Kramer et al. 2018), with recent observations suggesting that water maser flares can accompany ejection events associated with accretion bursts in massive and intermediate-mass stars (e.g., MacLeod et al. 2018; Brogan et al. 2018; Chen et al. 2021; Bayandina et al. 2022). Hence, one might expect such water maser flares from FUors/EXors. We therefore investigate if our targets have experienced water maser flares.

Figure 7 presents long-term time series for the water masers detected in our survey, which show that these masers are quite variable in both flux density and LSR velocity. Based on data from the literature, Z CMa appears to be in a relatively active phase, with the flux density of 2.4 Jy during our observations the highest observed to date (c.f. Blitz & Lada 1979; Thum et al. 1981; Deguchi et al. 1989; Scappini et al. 1991; Palla & Prusti 1993; Moscadelli et al. 2006; Sunada et al. 2007; Bae et al. 2011; Kim et al. 2018). For HH 354 IRS, no water maser emission was detected by previous observations (Wouterloot et al. 1993; Persi et al. 1994; Sunada et al. 2007). We report the first water maser detection toward this source. Since the upper limits of previous observations are comparable to the detected flux densities (see Figure 7), we cannot conclude whether the maser was in its active or quiescent phase during our observations. For V512 Per, Figure 7 compares the velocity component in our observations that likely arises from V512 Per (see Sect. 3.2.1) to archival data that include both single-dish and interferometric measurements (Haschick et al. 1980; Claussen et al. 1996; Rodríguez et al. 2002; Furuya et al. 2003). We note that in the case of the Claussen et al. (1996) data, the results were measured from the published figures. Based on this comparison, we identify three water maser flares, in 1978, 1992, and 1998, which reached peak flux densities of $\sim 310 \text{ Jy}$, 660 Jy , and 244 Jy on 1978 February 17, 1992 November 28, and 1998 June 22, respectively. The observations spanning these dates were performed with single-dish telescopes with large beams ($> 1'$), so H₂O(B) could potentially contribute to the observed flux densities (see Sect. 3.2.1). Claussen et al. (1996) note, however, that the maser features detected in their 1991-92 observations all had velocities consistent with those of H₂O(A)/V512 Per, suggesting that this flare was associated with the eruptive star.

For H₂O(B), we find no suggestion in the literature of this source being an eruptive variable at optical or near-infrared wavelengths, but our comparison with previous water maser observations (Figure 7; Haschick et al. 1980; Lyo et al. 2014) shows three maser flares with peak flux densities of $> 100 \text{ Jy}$, on 1975 November 30, 2012 May 28, and 2022 February 5. As for V512 Per, Figure 7 compares the velocity components in our observations that likely arise from H₂O(B) (Sect. 3.2.1&3.3.1) with historical data. Again, the large single dish beams encompass both H₂O(B) and V512 Per, meaning that we cannot rule out a contribution from V512 Per to the historical flares. For instance, the observations of Lyo et al. (2014) had a HPBW of $120''$. As noted in Sect. 3.3.1, the water maser flare detected in our observations on 2022 February 5 is the brightest to date, with a peak flux density of 498.7 Jy .

For IRAS 00338+6312, there is similarly no suggestion in the literature of this being an eruptive source in the optical or near-infrared, but Figure 7 suggests its water maser emission was in an active phase in 1998 and 2004 (Cesaroni et al. 1988; Henning et al. 1992; Wouterloot et al. 1993; Persi et al. 1994; Fiebig

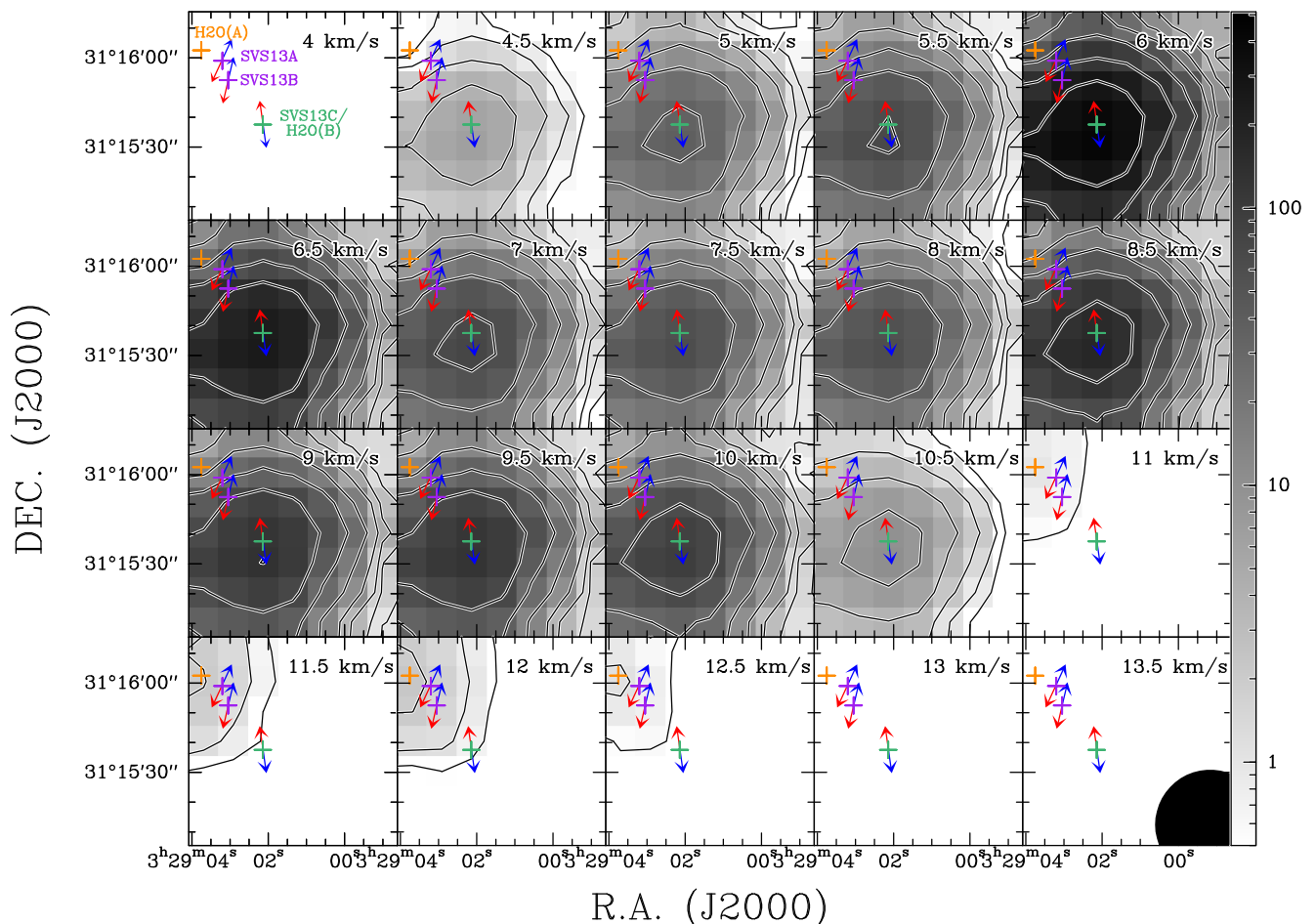


Fig. 5: Channel maps of H₂O masers in H₂O(B) (SVS 13C) and V512 Per (SVS 13A). The contours start at 0.5 Jy, and then increase by a factor of two. The plus signs represent the positions of the two H₂O masers (orange and green) previously detected by Haschick et al. (1980) and YSOs (purple; e.g., Plunkett et al. 2013). Based on previous observations (Plunkett et al. 2013; Podio et al. 2021), the outflow directions are indicated by red and blue arrows. The beam size is shown in the lower right corner of the last panel. The colour bar represents the flux density in units of Jy.

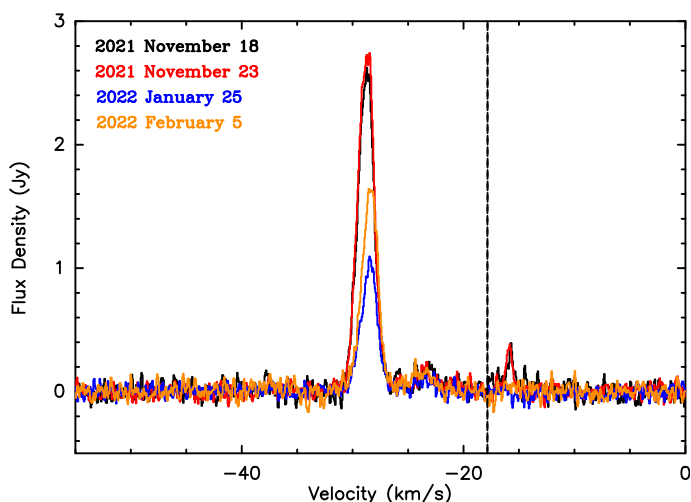


Fig. 6: H₂O maser observed in IRAS 00338+6312 at four epochs in 2021 November, 2022 January and February. The dashed vertical line indicates the systemic v_{LSR} of -17.83 km s^{-1} derived from the NH₃ (1,1), (2,2) and (3,3) transitions (Szabó et al. 2023).

1995; Codella et al. 1995; Furuya et al. 2003; Sunada et al. 2007; Bae et al. 2011), but relatively quiescent during our observations. The highest flux density reached was $\sim 31 \text{ Jy}$ on 1998 January 5 (Furuya et al. 2003).

Periodic variations have been reported in some velocity components of the 22.2 GHz H₂O (and the 6.7 GHz Class II CH₃OH) masers associated with the intermediate-mass YSO G107.298+5.639, and cyclic accretion instabilities have been invoked to explain this peculiar behavior (Szymczak et al. 2016). Low-mass stars like FUors and EXors might also experience cyclic accretion events, but we do not find evidence for periodic variations in Figure 7.

4.2. Scarcity of water masers in selected eruptive systems

Our water maser detection rate of 6% in FUors and EXors is perhaps surprising in light of the close connection between water maser emission and mass accretion and ejection in protostars (see Sect. 1). In this section, we consider possible explanations for the low detection rate.

First, the low detection rate could be caused by an evolutionary effect. Previous observations indicate that the water maser detection rate decreases from Class 0 to Class II objects (e.g., Furuya et al. 2001). Since the selected FUors/EXors are mainly

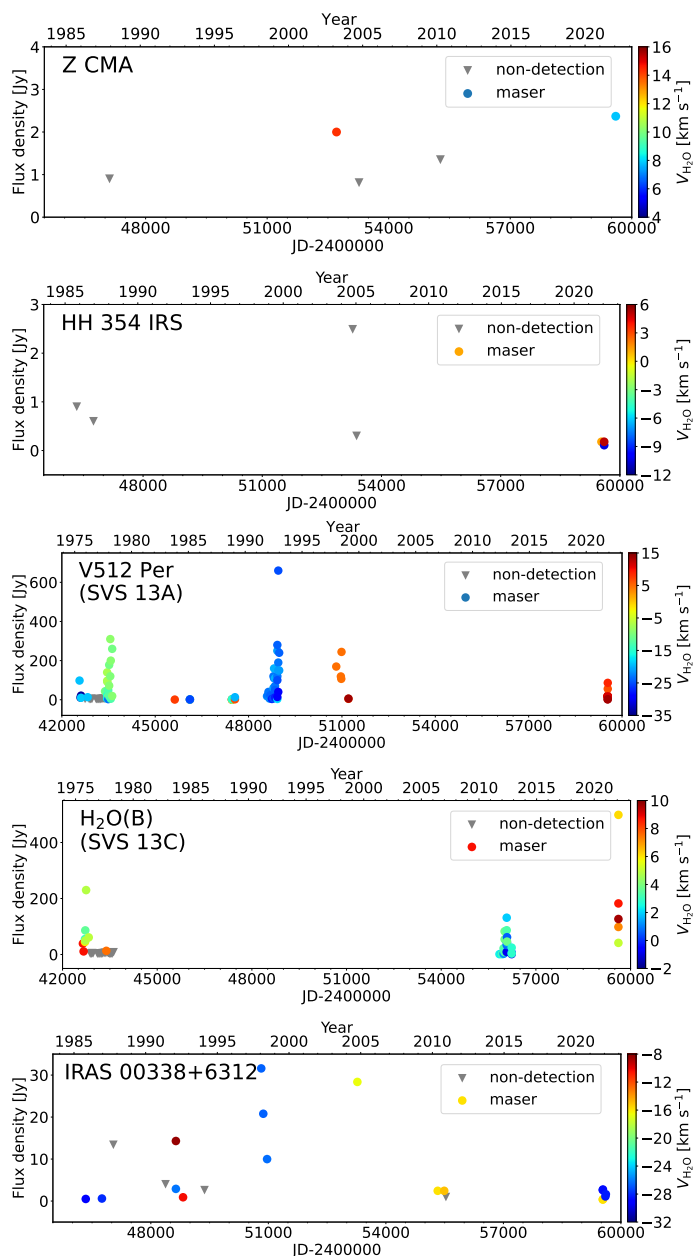


Fig. 7: Long-term variations in flux density of detected water masers. The colour-coded dots and grey triangles represent flux densities for maser detections, colour-coded by velocity (see colour-bar at right), and upper limits for non-detections, respectively. References for archival data are given in Sect. 4.1.

Class I and Class II objects (see Tables 1 and B.1), one would expect a lower detection rate compared to Class 0 objects. Furthermore, our detection rate is comparable to that (6.3%) for Class I objects in Furuya et al. (2001). We do not detect any water masers toward Class II objects, which further supports the evolutionary trend proposed by Furuya et al. (2001).

Second, water masers have relatively low luminosities in low-mass star formation regions. Statistical studies have shown that the maser luminosities are correlated with bolometric luminosities (e.g., Figure 16 in Urquhart et al. 2011). This suggests lower maser luminosities in low-mass star formation regions, so lower flux densities would be expected. This could contribute to our low detection rate toward low-mass eruptive stars. This is

supported by previous water maser surveys toward the Serpens South and Orion molecular clouds (Kang et al. 2013; Ortiz-León et al. 2021), which give detection rates of $\lesssim 2\%$ for low-mass protostars.

Third, water masers show rapid time variations. The time variability of water masers is evident in our study (see also Figures 2, 4 and 7). Water masers can be in a quiescent phase for ~ 5 years (Claussen et al. 1996), meaning that maser emission would not be detected during that time even for sources known to be associated with water masers. This is consistent with the fact that several water masers reported by previous studies are not detected in our observations (see Table B.1). It is possible that non-detection of water masers is due to their inactive state. Indeed, including historical detections, the detection rate of water masers in eruptive stars in our sample is $\sim 15\%$ (excluding the unclassified Gaia alerts), which is higher than our survey detection rate of 6%, suggesting that previously detected water masers were in an inactive phase during our observations.

5. Conclusions

In this paper, we presented the results of the first dedicated water maser survey towards FUors and EXors, two classes of low-mass young eruptive stars. We detected H_2O masers toward five objects, of which three are young eruptive stars: Z CMA (FUor; Class I), HH 354 IRS (FUor; Class 0/I), V512 Per (EXor; Class I), IRAS 00338+6312 (Class 0) and $\text{H}_2\text{O(B)}$ (Class 0). Our detection is the first report of water maser emission in HH 354 IRS. Our observations reveal the highest peak flux density yet reported towards $\text{H}_2\text{O(B)}$ (498.7 Jy), indicative of a recent H_2O maser flare. Overall, our observations result in a detection rate of $\sim 6\%$ for young eruptive stars. Analysis of the long-term time series of the water masers suggests that V512 Per and $\text{H}_2\text{O(B)}$ have experienced multiple water maser flares.

Despite the low detection rate, our observations have confirmed the presence of 22.2 GHz water maser emission in FUors and EXors, meaning that follow-up radio interferometric observations can be used to probe the environments of eruptive stars on small scales (see, e.g., Haschick et al. 1980; Rodríguez et al. 2002). If water masers are in general weak in FUors/EXors (Sect. 4.2), deeper observations would also be expected to find more of them. Expanding on optical and near-infrared knowledge of FUors/EXors with more radio observations, especially future VLBI measurements, will be crucial to better understand the underlying physics (e.g., mass accretion and ejection) of such peculiar objects, and eventually the formation of Sun-like stars.

Acknowledgements. We thank the referee for their valuable comments and suggestions which improved the quality of the manuscript. Based on observations (Project ID: 95-21, PI: Szabó) with the 100-m telescope of the MPIfR (Max-Planck-Institut für Radioastronomie) in Effelsberg. Zs.M.Sz. acknowledges funding from a St Leonards scholarship from the University of St Andrews. For the purpose of open access, the author has applied a Creative Commons Attribution (CC BY) licence to any Author Accepted Manuscript version arising. This project has received funding from the European Research Council (ERC) under the European Union's Horizon 2020 research and innovation programme under grant agreement No 716155 (SACCRED). This work has made use of the database for astrophysical masers⁴ (Ladeyschikov et al. 2022). O.B. acknowledges financial support from the Italian Ministry of University and Research - Project Proposal CIR01_00010. We acknowledge ESA Gaia, DPAC and the Photometric Science Alerts Team (<http://gsaweb.ast.cam.ac.uk/alerts>). This work presents results from the European Space Agency (ESA) space mission Gaia. Gaia data are being processed by the Gaia Data Processing and Analysis Consortium (DPAC). Funding for the DPAC is provided by national institutions, in particular the institutions participating in the Gaia MultiLateral Agreement

⁴ <https://maserdb.net/>

(MLA). The Gaia mission website is <https://www.cosmos.esa.int/gaia>. The Gaia archive website is <https://archives.esac.esa.int/gaia>.

References

- Ábrahám, P., Kóspál, Á., Kun, M., et al. 2018, *ApJ*, 853, 28
- Abraham, Z., Cohen, N. L., Opher, R., Raffaelli, J. C., & Zisk, S. H. 1981, *A&A*, 100, L10
- Anglada, G., Estalella, R., Pastor, J., Rodríguez, L. F., & Haschick, A. D. 1996, *ApJ*, 463, 205
- Anglada, G., Rodríguez, L. F., Girart, J. M., Estalella, R., & Torrelles, J. M. 1994, *ApJ*, 420, L91
- Anglada, G., Rodríguez, L. F., & Torrelles, J. M. 2000, *ApJ*, 542, L123
- Audard, M., Ábrahám, P., Dunham, M. M., et al. 2014, in *Protostars and Planets VI*, ed. H. Beuther, R. S. Klessen, C. P. Dullemond, & T. Henning, 387
- Bachiller, R., Gueth, F., Guilloteau, S., Tafalla, M., & Dutrey, A. 2000, *A&A*, 362, L33
- Bae, J.-H., Kim, K.-T., Youn, S.-Y., et al. 2011, *ApJS*, 196, 21
- Bailer-Jones, C. A. L., Rybizki, J., Founesneau, M., Demleitner, M., & Andrae, R. 2021, *AJ*, 161, 147
- Bailer-Jones, C. A. L., Rybizki, J., Founesneau, M., Mantelet, G., & Andrae, R. 2018, *AJ*, 156, 58
- Banzatti, A., Meyer, M. R., Manara, C. F., Pontoppidan, K. M., & Testi, L. 2014, *ApJ*, 780, 26
- Bayandina, O. S., Brogan, C. L., Burns, R. A., et al. 2022, *A&A*, 664, A44
- Blitz, L. & Lada, C. J. 1979, *ApJ*, 227, 152
- Boboltz, D. A., Simonetti, J. H., Dennison, B., Diamond, P. J., & Uphoff, J. A. 1998, *ApJ*, 509, 256
- Bonnefoy, M., Chauvin, G., Dougados, C., et al. 2017, *A&A*, 597, A91
- Brand, J., Wouterloot, J. G. A., Codella, C., Massi, F., & Giannetti, A. 2019, *A&A*, 628, A98
- Brogan, C. L., Hunter, T. R., Cyganowski, C. J., et al. 2018, *ApJ*, 866, 87
- Bronfman, L., Nyman, L. A., & May, J. 1996, *A&AS*, 115, 81
- Burns, R. A., Handa, T., Nagayama, T., Sunada, K., & Omodaka, T. 2016, *MNRAS*, 460, 283
- Cesaroni, R., Palagi, F., Felli, M., et al. 1988, *A&AS*, 76, 445
- Chen, X., Arce, H. G., Zhang, Q., et al. 2013, *ApJ*, 768, 110
- Chen, Z., Sun, W., Chini, R., et al. 2021, *ApJ*, 922, 90
- Claussen, M. J., Wilking, B. A., Benson, P. J., et al. 1996, *ApJS*, 106, 111
- Codella, C., Palumbo, G. G. C., Pareschi, G., et al. 1995, *MNRAS*, 276, 57
- Connelley, M. S. & Greene, T. P. 2010, *AJ*, 140, 1214
- Connelley, M. S. & Reipurth, B. 2018, *ApJ*, 861, 145
- Cruz-Sáenz de Miera, F., Kóspál, Á., Ábrahám, P., et al. 2022, *ApJ*, 927, 125
- Cyganowski, C. J., Koda, J., Rosolowsky, E., et al. 2013, *ApJ*, 764, 61
- Deguchi, S., Nakada, Y., & Forster, J. R. 1989, *MNRAS*, 239, 825
- Díaz-Rodríguez, A. K., Anglada, G., Blázquez-Calero, G., et al. 2022, *ApJ*, 930, 91
- Dong, R., Liu, H. B., Cuello, N., et al. 2022, *Nature Astronomy*, 6, 331
- Eisloffel, J., Guenther, E., Hessman, F. V., et al. 1991, *ApJ*, 383, L19
- Elitzur, M. 1992, *ARA&A*, 30, 75
- Elitzur, M. & Fuqua, J. B. 1989, *ApJ*, 347, L35
- Elitzur, M., Hollenbach, D. J., & McKee, C. F. 1989a, *ApJ*, 346, 983
- Elitzur, M., Hollenbach, D. J., & McKee, C. F. 1989b, *ApJ*, 346, 983
- Evans, Neal J. I., Dunham, M. M., Jørgensen, J. K., et al. 2009, *ApJS*, 181, 321
- Fehér, O., Kóspál, Á., Ábrahám, P., Hogerheijde, M. R., & Brinch, C. 2017, *A&A*, 607, A39
- Felli, M., Palagi, F., & Tofani, G. 1992, *A&A*, 255, 293
- Fiebig, D. 1995, *A&A*, 298, 207
- Fiebig, D., Duschl, W. J., Menten, K. M., & Tscharnuter, W. M. 1996, *A&A*, 310, 199
- Fischer, W. J., Hillenbrand, L. A., Herczeg, G. J., et al. 2022, *Protostars and Protoplanets VII*, arXiv:2203.11257
- Fujiyoshi, T., Wright, C. M., & Moore, T. J. T. 2015, *MNRAS*, 451, 3371
- Fuller, G. A., Ladd, E. F., Padman, R., Myers, P. C., & Adams, F. C. 1995, *ApJ*, 454, 862
- Furuya, R. S., Kitamura, Y., Wootten, A., Claussen, M. J., & Kawabe, R. 2003, *ApJS*, 144, 71
- Furuya, R. S., Kitamura, Y., Wootten, H. A., Claussen, M. J., & Kawabe, R. 2001, *ApJ*, 559, L143
- Gaia Collaboration. 2022, *VizieR Online Data Catalog*, I/355
- Giannini, T., Lorenzetti, D., Antonucci, S., et al. 2016, *ApJ*, 819, L5
- Gildas Team. 2013, *GILDAS: Grenoble Image and Line Data Analysis Software*
- Gómez, J. F., de Gregorio-Monsalvo, I., Suárez, O., & Kuiper, T. B. H. 2006, *AJ*, 132, 1322
- Goodrich, R. W. 1986, *AJ*, 92, 885
- Gramajo, L. V., Rodón, J. A., & Gómez, M. 2014, *AJ*, 147, 140
- Gray, M. 2012, *Maser Sources in Astrophysics*, book published by the Cambridge University Press
- Gray, M. D., Etoka, S., Richards, A. M. S., & Pimpanuwat, B. 2022, *MNRAS*, 513, 1354
- Greene, T. P., Wilking, B. A., Andre, P., Young, E. T., & Lada, C. J. 1994, *ApJ*, 434, 614
- Hartmann, L. & Kenyon, S. J. 1996, *ARA&A*, 34, 207
- Haschick, A. D., Moran, J. M., Rodríguez, L. F., et al. 1980, *ApJ*, 237, 26
- Henning, T., Cesaroni, R., Walmsley, M., & Pfau, W. 1992, *A&AS*, 93, 525
- Herbig, G. H. 1977, *ApJ*, 217, 693
- Herbig, G. H. 1989, in *European Southern Observatory Conference and Workshop Proceedings*, Vol. 33, *European Southern Observatory Conference and Workshop Proceedings*, title of the workshop: "ESO Workshop on Low Mass Star Formation and Pre-Main sequence objects", 233–246
- Herbig, G. H. 1990, *ApJ*, 360, 639
- Hillenbrand, L. A., Miller, A. A., Covey, K. R., et al. 2013, *AJ*, 145, 59
- Hirota, T., Tsuboi, M., Fujisawa, K., et al. 2011, *ApJ*, 739, L59
- Hodgkin, S. T., Harrison, D. L., Breedt, E., et al. 2021, *A&A*, 652, A76
- Hunter, T. R., Taylor, G. B., Felli, M., & Tofani, G. 1994, *A&A*, 284, 215
- Jurdana-Šepić, R., Munari, U., Antonucci, S., Giannini, T., & Lorenzetti, D. 2018, *A&A*, 614, A9
- Kang, M., Lee, J.-E., Choi, M., et al. 2013, *ApJS*, 209, 25
- Kazarovets, E. V., Samus, N. N., & Goranskij, V. P. 1993, *Information Bulletin on Variable Stars*, 3840, 1
- Kenyon, S. J., Hartmann, L., Gomez, M., Carr, J. S., & Tokunaga, A. 1993, *AJ*, 105, 1505
- Kim, C.-H., Kim, K.-T., & Park, Y.-S. 2018, *ApJS*, 236, 31
- Kim, J.-S., Kim, S.-W., Kurayama, T., et al. 2013, *ApJ*, 767, 86
- Klein, B., Hochgürtel, S., Krämer, I., et al. 2012, *A&A*, 542, L3
- Koresko, C. D., Beckwith, S. V. W., Ghez, A. M., Matthews, K., & Neugebauer, G. 1991, *AJ*, 102, 2073
- Kóspál, Á., Ábrahám, P., Acosta-Pulido, J. A., et al. 2016, *A&A*, 596, A52
- Kóspál, Á., Ábrahám, P., Apai, D., et al. 2008, *MNRAS*, 383, 1015
- Kóspál, Á., Ábrahám, P., Csengeri, T., et al. 2017, *ApJ*, 836, 226
- Kóspál, Á., Ábrahám, P., Moór, A., et al. 2015, *ApJ*, 801, L5
- Kramer, B. H., Menten, K. M., & Kraus, A. 2018, in *Astrophysical Masers: Unlocking the Mysteries of the Universe*, ed. A. Tarchi, M. J. Reid, & P. Castangia, Vol. 336, 279–280
- Ladeyschikov, D. A., Sobolev, A. M., Bayandina, O. S., & Shakhvorostova, N. N. 2022, *AJ*, 163, 124
- Lekht, E. E. & Sorochenko, R. L. 1984, *Soviet Astronomy Letters*, 10, 307
- Liu, H. B., Dunham, M. M., Pascucci, I., et al. 2018, *A&A*, 612, A54
- Lo, K. Y. & Bechis, K. P. 1973, *ApJ*, 185, L71
- Lo, K. Y. & Bechis, K. P. 1974, *ApJ*, 190, L125
- Lyo, A. R., Kim, J., Byun, D.-Y., & Lee, H.-G. 2014, *AJ*, 148, 80
- MacLeod, G. C., Smits, D. P., Goedhart, S., et al. 2018, *MNRAS*, 478, 1077
- Mathieu, R. D., Martin, E. L., & Magazzu, A. 1996, in *American Astronomical Society Meeting Abstracts*, Vol. 188, *American Astronomical Society Meeting Abstracts #188*, 60.05
- Mauron, N. & Thouvenot, E. 1991, *SVS* 13, <http://www.cbat.eps.harvard.edu/iauc/05200/05261.html>, iAUC 5261: 1991Z; SVS 13: 1991g
- Menten, K. M., Reid, M. J., Forbrich, J., & Brunthaler, A. 2007, *A&A*, 474, 515
- Miller, A. A., Hillenbrand, L. A., Bilgi, P., et al. 2015, *The Astronomer's Telegram*, 7428, 1
- Mookerjee, B., Ghosh, S. K., Karnik, A. D., et al. 1999, *Bulletin of the Astronomical Society of India*, 27, 155
- Moriarty-Schieven, G. H., Aspin, C., & Davis, G. R. 2008, *AJ*, 136, 1658
- Moscadelli, L., Sanna, A., Goddi, C., et al. 2019, *A&A*, 631, A74
- Moscadelli, L., Testi, L., Furuya, R. S., et al. 2006, *A&A*, 446, 985
- Nagy, Z., Szegedi-Elek, E., Ábrahám, P., et al. 2021, *MNRAS*, 504, 185
- Omodaka, T., Maeda, T., Miyoshi, M., et al. 1999, *PASJ*, 51, 333
- Ortiz-León, G. N., Plunkett, A. L., Loinard, L., et al. 2021, *AJ*, 162, 68
- Ott, M., Witzel, A., Quirrenbach, A., et al. 1994, *A&A*, 284, 331
- Palagi, F., Cesaroni, R., Comoretto, G., Felli, M., & Natale, V. 1993, *A&AS*, 101, 153
- Palla, F. & Prusti, T. 1993, *A&A*, 272, 249
- Park, S., Kóspál, Á., Ábrahám, P., et al. 2022, *ApJ*, 941, 165
- Park, S., Kóspál, Á., Cruz-Sáenz de Miera, F., et al. 2021, *ApJ*, 923, 171
- Parsamian, E. S. & Mujica, R. 2004, *Astrophysics*, 47, 433
- Persi, P., Palagi, F., & Felli, M. 1994, *A&A*, 291, 577
- Pety, J. 2005, in *SF2A-2005: Semaine de l'Astrophysique Française*, ed. F. Casoli, T. Contini, J. M. Hameury, & L. Pagani, 721
- Pickett, H. M., Poynter, R. L., Cohen, E. A., et al. 1998, *J. Quant. Spectr. Rad. Transf.*, 60, 883
- Plunkett, A. L., Arce, H. G., Corder, S. A., et al. 2013, *ApJ*, 774, 22
- Podio, L., Tabone, B., Codella, C., et al. 2021, *A&A*, 648, A45
- Principe, D. A., Cieza, L., Hales, A., et al. 2018, *MNRAS*, 473, 879
- Quanz, S. P., Henning, T., Bouwman, J., Linz, H., & Lahuis, F. 2007, *ApJ*, 658, 487
- Reid, M. J. & Honma, M. 2014, *ARA&A*, 52, 339
- Reipurth, B. & Aspin, C. 1997, *AJ*, 114, 2700

- Reipurth, B., Bally, J., & Devine, D. 1997, *AJ*, 114, 2708
- Rodríguez, L. F., Anglada, G., & Curiel, S. 1997, *ApJ*, 480, L125
- Rodríguez, L. F., Anglada, G., Torrelles, J. M., et al. 2002, *A&A*, 389, 572
- Ruiz-Rodríguez, D., Cieza, L. A., Williams, J. P., et al. 2017, *MNRAS*, 466, 3519
- Sandell, G. & Weintraub, D. A. 2001, *ApJS*, 134, 115
- Scappini, F., Caselli, P., & Palumbo, G. G. C. 1991, *MNRAS*, 249, 763
- Segura-Cox, D. M., Looney, L. W., Tobin, J. J., et al. 2018, *ApJ*, 866, 161
- Snell, R. L., Dickman, R. L., & Huang, Y. L. 1990, *ApJ*, 352, 139
- Staude, H. J. & Neckel, T. 1991, *A&A*, 244, L13
- Stecklum, B., Melnikov, S. Y., & Meusinger, H. 2007, *A&A*, 463, 621
- Strom, S. E., Vrba, F. J., & Strom, K. M. 1976, *AJ*, 81, 314
- Sunada, K., Nakazato, T., Ikeda, N., et al. 2007, *PASJ*, 59, 1185
- Szabó, Z. M., Gong, Y., Menten, K. M., et al. 2023, *A&A*, 672, A158
- Szegedi-Elek, E., Ábrahám, P., Wyrzykowski, L., et al. 2020, *ApJ*, 899, 130
- Szymczak, M., Olech, M., Wolak, P., Bartkiewicz, A., & Gawroński, M. 2016, *MNRAS*, 459, L56
- Takaba, H., Iwata, T., Miyaji, T., & Deguchi, S. 2001, *Communications Research Laboratory Review*, 47, 107
- Takami, M., Chen, T.-S., Liu, H. B., et al. 2019, *ApJ*, 884, 146
- Thum, C., Bertout, C., & Downes, D. 1981, *A&A*, 94, 80
- Urquhart, J. S., Hoare, M. G., Lumsden, S. L., et al. 2009, *A&A*, 507, 795
- Urquhart, J. S., Morgan, L. K., Figura, C. C., et al. 2011, *MNRAS*, 418, 1689
- Valdettaro, R., Palla, F., Brand, J., et al. 2001, *A&A*, 368, 845
- Visser, A. E., Richer, J. S., & Chandler, C. J. 2002, *AJ*, 124, 2756
- Wachmann, A. 1954, *ZAp*, 35, 74
- White, J. A., Kóspál, Á., Rab, C., et al. 2019, *ApJ*, 877, 21
- Winkel, B., Kraus, A., & Bach, U. 2012, *A&A*, 540, A140
- Winnberg, A., Graham, D., Walmsley, C. M., & Booth, R. S. 1981, *A&A*, 93, 79
- Wouterloot, J. G. A., Brand, J., & Fiegle, K. 1993, *A&AS*, 98, 589
- Yang, J., Umemoto, T., Iwata, T., & Fukui, Y. 1991, *ApJ*, 373, 137
- Yung, B. H. K., Nakashima, J.-i., Imai, H., et al. 2013, *ApJ*, 769, 20
- Zapata, L. A., Galván-Madrid, R., Carrasco-González, C., et al. 2015, *ApJ*, 811, L4
- Zsidi, G., Ábrahám, P., Acosta-Pulido, J. A., et al. 2019, *ApJ*, 873, 130
- Zurlo, A., Cieza, L. A., Williams, J. P., et al. 2017, *MNRAS*, 465, 834

Appendix A: W75N

During our initial observing run on 2021 November 18, our setup was verified by observing W75N, a well-known massive star-forming region showing bright water masers (Lekht & Sorochenko 1984; Hunter et al. 1994; Kim et al. 2013, and references therein). Although our survey focused on low- and intermediate-mass young stars, here we briefly present the W75N maser spectrum to make it available for potential future studies of maser variability in this region. Figure A.1 shows the water maser spectrum observed toward W75N on 2021 November 18. The dashed vertical line indicates the average centroid v_{LSR} of 9.43 km s⁻¹ derived from the NH₃ (1,1), (2,2) and (3,3) transitions. In Table A.1, we list the properties of the water maser features, along with the v_{LSR} results from the NH₃ transitions.

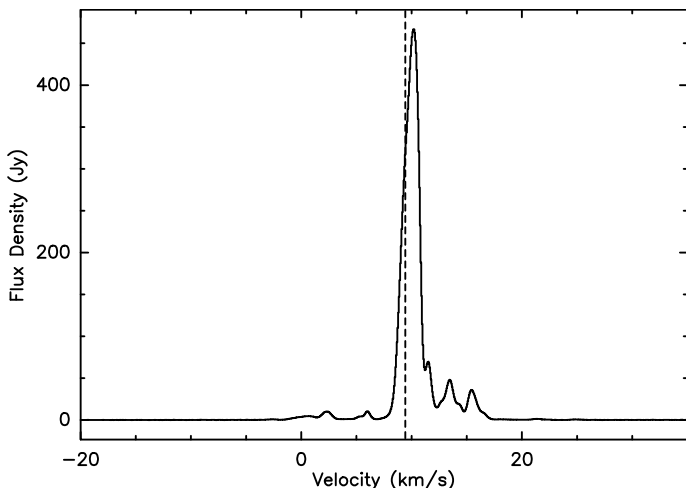


Fig. A.1: H₂O maser spectrum observed toward W75N on 2021 November 18. The dashed line indicates the centroid LSR velocity of 9.43 km s⁻¹ from the NH₃ (1,1), (2,2) and (3,3) transitions.

Table A.1: H₂O maser velocity components and NH₃ LSR velocities from observations of W75N on 2021 November 18.

H ₂ O				NH ₃ (1,1) – (2,2) – (3,3)		
v_{LSR} (km s ⁻¹)	RMS (Jy)	S_{ν}^* (Jy)	$L_{\text{H}_2\text{O}}$ (L _⊙)	v_{LSR} (km s ⁻¹)	v_{LSR} (km s ⁻¹)	v_{LSR} (km s ⁻¹)
0.84 (0.01)	0.08	11.27	3.06×10 ⁻⁶			
5.88 (1.23)	0.08	11.27	3.91×10 ⁻⁷			
9.99 (0.03)	0.08	467.64	3.23×10 ⁻⁵	9.48 (0.03)	9.37 (0.04)	9.46 (0.07)
13.35 (0.06)	0.08	49.71	3.11×10 ⁻⁶			
15.56 (0.06)	0.08	36.50	1.32×10 ⁻⁶			

Notes. *Results from the Gaussian fitting, for more information, see Sect. 2.

Appendix B: Non-detections in our survey

In total, our survey consisted of 51 objects: 33 FUors, 13 EXors and 5 Gaia alerts accessible with the Effelsberg 100-m telescope. The chosen Gaia alerts are part of the Piskésetető Monitoring Program, in Hungary, which started a few years ago with the aim of following the optical wavelength brightness variations of Gaia alert sources with light curves that resemble those of FUors and EXors (see e.g., Szegedi-Elek et al. 2020; Nagy et al. 2021; Cruz-Sáenz de Miera et al. 2022). We chose Gaia alerts for inclusion in our sample based on their having light curves and lumi-

nositities similar to those of FUors and EXors. Water masers were detected in only four out of our 51 targeted sources, however the emission in one of those target pointings is not attributed to the targeted eruptive star (see Sect. 3.3.2). The 48 non-detections, within an expected velocity range from -100 to +100 km s⁻¹, are reported in Table B.1.

Table B.1: H₂O maser non-detections in our survey.

Source	Type (FUor/EXor/ Gaia alert)	R.A. (J2000) (^h ^m ^s)	Dec. (J2000) ([°] ['] ^{''})	Upper limit ^(a) (Jy)	Previous survey ^(b) (No/Yes/ Unknown)	Date ^(c) (A/B/C)	Classification (Class 0 – II)	Ref.	D ^(d) (pc)
V1180 Cas	EXor	02 33 01.53	+72 43 26.8	0.17	Unk.		–	–	908 [51]
PP 13S	FUor	04 10 41.09	+38 07 54.5	0.18	Yes [1]		I	21	350
L1551 IRS 5	FUor	04 31 34.07	+18 08 04.9	0.17	No [2,3]		I	22	–
XZ Tau	EXor	04 31 40.08	+18 13 56.6	0.18	Unk.		II	23	140
UZ Tau E	EXor	04 32 43.02	+25 52 30.9	0.18	Unk.		II	24	130 [51]
LDN 1415 IRS	EXor	04 41 37.50	+54 19 22.0	0.21	Unk.		I	25	170
DR Tau	EXor	04 47 06.21	+16 58 42.8	0.17	Unk.		II	26	192 [51]
V582 Aur	FUor	05 25 51.97	+34 52 30.0	0.15	Unk.		II	27	2401 [52,53]
V1118 Ori	EXor	05 34 44.98	–05 33 41.3	0.21	Unk.		II	28	414
Haro 5a IRS	FUor	05 35 26.74	–05 03 55.0	0.21	Unk.		0/I	29	450
NY Ori	EXor	05 35 36.00	–05 12 25.2	0.22	Unk.		–	–	403 [51]
V1143 Ori	EXor	05 38 03.89	–04 16 42.8	0.22	Unk.		II	30	395 [51]
V883 Ori	FUor	05 38 18.09	–07 02 25.9	0.20	No [4,5]		I	31	417 [54]
HBC 494	FUor	05 40 27.45	–07 27 30.0	0.21	Unk.		I	32	–
V2775 Ori	FUor	05 42 48.48	–08 16 34.7	0.25	No [6]		late I	33	420
FU Ori	FUor	05 45 22.37	+09 04 12.3	0.22	Unk.		II	34	407 [51]
V1647 Ori	FUor	05 46 13.13	–00 06 04.8	0.23	Unk.	A	I/II	35	412 [51]
AR 6A/6B	FUor	06 40 59.30	+09 35 49.0	0.23	Unk.		II	36	800
Parsamian 21	FUor	19 29 00.84	+09 38 43.4	0.16	Unk.		I/II	37	400
I 18270-0153W	FUor	18 29 36.90	–01 51 02.0	0.19	No [7]		I	38	–
OO Ser	FUor	18 29 49.13	+01 16 20.6	0.18	No [3,8]		I	38	311
V371 Ser	EXor	18 29 51.21	+01 16 39.4	0.18	No [3,8]		–	–	311
Gaia21aul	Gaia alert	18 30 06.18	00 42 33.30	0.17	No [9,10]		–	–	378 [55]
I 18341-0113S	FUor	18 36 45.70	–01 10 29.0	0.19	No [3,7]		I	38	–
Gaia21aru	Gaia alert	19 00 56.41	18 48 29.20	0.16	Unk.		–	–	–
V1515 Cyg	FUor	20 23 48.01	+42 12 25.7	0.18	Unk.		–	–	900 [55]
PV Cep	EXor	20 45 53.90	+67 57 38.6	0.17	Yes [5,11]		–	–	325
					No [10,12,13,14,15]				
V2492 Cyg	EXor	20 51 26.23	+44 05 23.8	0.16	No [16]		I	39	804 [51]
V1057 Cyg	FUor	20 58 53.73	+44 15 28.4	0.17	Yes [11]		II	40	891 [55]
					No [3,10,12,13,14]				
HBC 722	FUor	20 58 17.00	+43 53 43.0	0.17	Unk.		II	41	757 [55]
V2495 Cyg	FUor	21 00 25.24	+52 30 16.9	0.16	No [9]		I/II	42	800
RNO 127	FUor	21 00 31.80	+52 29 17.0	0.17	Unk.		–	–	800
CB 230	FUor	21 17 38.62	+68 17 34.0	0.15	No [3,7,17,18]		0/I	43	339 [18]
V1735 Cyg	FUor	21 47 20.66	+47 32 03.8	0.18	No [1,3,12]		II	43	663 [55]
V733 Cep	FUor	22 53 33.25	+62 32 23.6	0.16	Unk.		I/II	43	724 [55]
VY Tau	EXor	04 39 17.42	+22 47 53.3	0.11	Unk.		II	44	153 [55]
Gaia21arx	Gaia alert	05 36 24.80	–06 17 30.52	0.15	Unk.		–	–	361 [55]
NGC 2071	FUor	05 47 09.80	+00 18 00.0	0.15	Yes [1,3,6]		–	–	–
I 06297+1021W	FUor	06 32 28.70	+10 19 0	0.16	Unk.	B	I	43	–
I 06393+0913	FUor	06 42 08.13	+09 10 30.0	0.15	Unk.		I	43	–
Gaia18dvy	FUor	20 05 06.02	+36 29 13.52	0.14	Unk.		II	45	1880 [45]
Gaia19bpg	Gaia alert	21 41 50.43	+51 55 45.48	0.12	Unk.		–	–	–
V899 Mon	FUor	06 09 19.24	–06 41 55.8	0.10	Unk.		II	46	809 [51]
V900 Mon	FUor	06 57 22.22	–08 23 17.6	0.13	Unk.		I	47	1304 [51]
V960 Mon	FUor	06 59 31.58	–04 05 27.7	0.12	Unk.	C	II	48	2189 [51]
iPTF 15AFQ	FUor	07 09 21.39	–10 29 34.5	0.13	Unk.		I	49	1315 [51]
Gaia20bdb	Gaia alert	07 10 14.92	–18 27 01.04	0.15	Unk.		–	–	–
				0.05		A			
				0.04		B			
RNO 1B/1C	FUor	00 36 46.30	+63 28 54.0	0.04	No [1,7,8,10,19,20]		1B: 0/I–II, 1C: II	50	965 [55]
				0.04		C			
				0.05		D			

Notes. Source types and coordinates are taken from Audard et al. (2014), except for Gaia alerts, for which positions are taken from the Gaia alerts system. ^(a) Upper limits are $3 \times \text{RMS}$. ^(b) Previous surveys: No – Source was observed, but no H₂O maser detected; Yes – H₂O maser detected; Unk. (Unknown) – To our knowledge, previously not searched for water masers.

^(c) Our observations were carried out on: A – 2021-11-18; B – 2021-11-23; C – 2022-01-25.; D – 2022-02-05. ^(d) Distance – the default values are from Audard et al. (2014), but in case of more recent data (i.e. Gaia), the values are then updated with references.

References: 1 – Wouterloot et al. (1993); 2 – Claussen et al. (1996); 3 – Sunada et al. (2007); 4 – Deguchi et al. (1989); 5 – Takaba et al. (2001); 6 – Kang et al. (2013); 7 – Codella et al. (1995); 8 – Furuya et al. (2003); 9 – Yung et al. (2013); 10 – Bae et al. (2011); 11 – Cesaroni et al. (1988); 12 – Felli et al. (1992); 13 – Palagi et al. (1993); 14 – Palla & Prusti (1993); 15 – Valdetaro et al. (2001); 16 – Urquhart et al. (2011); 17 – Gómez et al. (2006); 18 – Brand et al. (2019); 19 – Henning et al. (1992); 20 – Fiebig (1995); 21 – Sandell & Weintraub (2001); 22 – Fuller et al. (1995); 23 – Zapata et al. (2015); 24 – Mathieu et al. (1996); 25 – Stecklum et al. (2007); 26 – Banzatti et al. (2014); 27 – Ábrahám et al. (2018); 28 – Giannini et al. (2016); 29 – Kóspál et al. (2017); 30 – Parsamian & Mujica (2004); 31 – White et al. (2019); 32 – Ruíz-Rodríguez et al. (2017); 33 – Zurlo et al. (2017); 34 – Herbig (1977); 35 – Principe et al. (2018); 36 – Moriarty-Schieven et al. (2008); 37 – Kóspál et al. (2008); 38 – Connelley & Greene (2010); 39 – Hillenbrand et al. (2013); 40 – Fehér et al. (2017); 41 – Kóspál et al. (2016); 42 – Liu et al. (2018); 43 – Connelley & Reipurth (2018); 44 – Herbig (1990); 45 – Szegedi-Elek et al. (2020); 46 – Park et al. (2021); 47 – Takami et al. (2019); 48 – Kóspál et al. (2015); 49 – Miller et al. (2015); 50 – Quanz et al. (2007); 51 – Gaia Collaboration (2022); 52 – Bailer-Jones et al. (2018); 53 – Zsidi et al. (2019); 54 – Menten et al. (2007); 55 – Bailer-Jones et al. (2021)